Wear 269 (2010) 416–423

Contents lists available at ScienceDirect

Wear

journal homepage: www.elsevier.com/locate/wear

The effect of laser polishing on fretting wear between a hemisphere and a flat plate

B. Raeymaekers*, F.E. Talke

University of California San Diego, 9500 Gilman Dr., La Jolla, CA 92093-0401, United States

ARTICLE INFO

Article history:
Received 25 August 2009
Received in revised form 23 April 2010
Accepted 28 April 2010
Available online 13 May 2010

Keywords:
Fretting
Wear
Laser polishing

ABSTRACT

Fretting wear between a hemisphere and a flat plate is investigated experimentally and the effect of laser polishing is studied. The energy dissipated between the hemisphere and the flat plate is determined as a function of operating conditions such as frequency and normal load and material properties such as surface roughness, and related to the wear observed at the sliding interface. Abrasive, adhesive and tribochemical wear are formed on the hemisphere and flat plate. No significant difference in wear production between a laser polished and a regular stainless steel hemisphere was observed.

1. Introduction

Fretting is defined as a cyclic relative motion between two surfaces in contact at small displacement amplitude [1–3]. Depending on material properties, loading conditions and environment, fretting can cause fretting fatigue or fretting wear [4,5]. Mechanisms for fretting wear are oxidation, adhesion, surface fatigue or abrasion [6]. Fretting wear occurs in many instances where mechanical parts are in sliding contact. Specific situations where fretting wear can occur are for example electrical switches where contacting conductors make a reciprocating contact when the switch is operated. Other examples include structural elements of bridges which undergo reciprocal sliding against each other due to dynamic loading (e.g., traffic, weather), and turbo machinery such as jet engine fans, compressors and turbines. Fretting wear can cause critical mechanical components to fail with potentially catastrophic consequences. Abrasive elements such as dust particles and sand (e.g., desert environment for jet engines) accelerate fretting wear. Atmospheric factors such as a corrosive environment also accelerate fretting wear [7]. For example, intertwined cables that span or are submerged in a corrosive medium and which slide over each other in a reciprocal fashion are damaged and eventually fail as a result of fretting. Fretting wear also occurs at the nanoscale. The slider containing the read/write element which flies over a magnetic disk in a hard disk drive rubs against a dimple on the suspension, thereby creating a reciprocal contact that may create wear particles and cause the hard disk drive to fail. MEMS and NEMS type devices are also subject to fretting wear. Lastly, sliding interfaces of prosthetic implants and artificial body parts are also subject to reciprocal motion, and, thus, subject to failure as a result of fretting wear.

At present, very little information is available in the open literature concerning how surface roughness affects fretting wear and how surface treatments influence the wear created between two bodies in reciprocating sliding contact. This paper tries to address this gap by studying the effect of laser polishing on wear at the interface between a hemisphere and a flat in reciprocating motion. Additionally, this paper tries to match the obtained experimental data with existing fretting and traditional uni-directional sliding models available in the literature.

2. Fretting research

Experimental investigations have shown that cyclic motion at the contact interface between two bodies can be divided into four different regimes of sliding: stick, partial slip, gross slip and reciprocal sliding [8,9]. A detailed description of the four fretting regimes is provided in [8]. The fretting regimes can be characterized as a function of normal load and displacement amplitude using so-called "fretting maps" [8]. The transition from "fretting" to "reciprocal sliding" is independent of the normal load but depends on the displacement amplitude [8,10].

Varenberg et al. [11] introduced a so-called "slip index", a criterion to determine different fretting regimes from a friction force versus relative displacement (friction hysteresis loop) measurement of the reciprocal motion between two samples [11,12]. The

* Corresponding author. Fax: +1 858 534 2720.
E-mail address: bart@talkelab.ucsd.edu (B. Raeymaekers).

0043-1648/$ – see front matter © 2010 Elsevier B.V. All rights reserved.
doi:10.1016/j.wear.2010.04.027

Nomenclature

A_d	displacement amplitude
A_s	sliding amplitude
C_ν	ratio of maximum contact pressure under perfect slip condition at yield inception, and the yield strength
d_0	minimum separation between hemisphere and flat based on asperity heights
d_0^*	dimensionless minimum separation between hemisphere and flat based on asperity heights, d_0/σ
E	Young's modulus
H	hardness
h_0	minimum separation between hemisphere and flat based on surface heights
h^*	dimensionless minimum separation between hemisphere and flat based on surface heights h_0/σ
L_c	critical normal load under full stick condition
$\overline{L_c}$	ratio of the critical normal load under full stick condition and perfect slip, L_c/P_c
L_{eq}	equivalent sliding distance
n	number of fretting cycles
P	normal load
P^*	dimensionless normal load, P/L_c
P_c	critical normal load under slip condition
Q_{max}	maximum tangential load or friction force at sliding inception
Q^*_{max}	dimensionless maximum tangential load, Q_{max}/L_c
R	hemisphere radius of curvature
r	radial coordinate
r^*	dimensionless radial coordinate, $r/\sqrt{R\sigma}$
Y_0	yield strength
z	height of an asperity, based on the mean of asperity heights
z^*	dimensionless height of an asperity, z/σ
β	roughness parameter, $\rho\sigma_s\eta$
δ	slip index
δ_c	critical interference in stick
$\overline{\delta_c}$	ratio of the critical interferences in full stick and perfect slip, δ_c/ω_c
η	area density of asperities
μ	static friction coefficient
ν	Poisson coefficient
ρ	mean asperity tip radius of curvature
σ	standard deviation of asperity heights
σ_s	standard deviation of asperity summit heights
Φ^*	dimensionless distribution function of asperity heights
ψ	plasticity index
ω_c	critical interference in perfect slip

slip index δ is defined as

$$\delta = \frac{A_d S_c}{P} \tag{1}$$

where A_d is the displacement amplitude, A_s is the slip amplitude and S_c is the slope of the typical friction hysteresis loop, as illustrated in Fig. 1. P is the normal load.

The transition between the four sliding regimes for any given loading conditions can be specified by the slip index, which is universal for any scale from nano to macro fretting [12]. Varenberg identified the four regimes of sliding in terms of the slip index. Reciprocal sliding was found to occur when $\delta > 11$ and fretting was restricted to $\delta < 10$. Gross slip was found between $0.8 < \delta < 10$ and partial slip between $0.5 < \delta < 0.6$. The regime $\delta < 0.5$ was suggested to correspond to stick, pending more experimental validation.

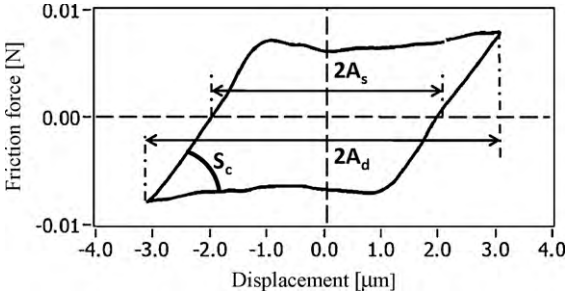

Fig. 1. Friction hysteresis loop definitions.

3. Experimental apparatus

Fig. 2(a) shows a schematic of the experimental apparatus used in this study. The set up consists of a shear mode piezo (PZT) actuator and a beam with a hemispherical shape punched into its surface, and is similar to several fretting testers documented in the literature [e.g., 13]. The beam is attached to a strain gauge-based load cell and positioned adjacent to the shear mode PZT. The hemisphere rests on the test specimen (flat plate), which is attached to a shear mode piezo (PZT) actuator, applying the tangential reciprocating loading. A normal force P is applied to the dimple by means of a dead weight. The shear mode PZT is actuated with a triangularly shaped input voltage signal with constant amplitude from a signal generator to create a reciprocating motion between the hemisphere and the test specimen. The displacement of the PZT actuator (see Fig. 2(c)) is measured with an optical displacement sensor. The load cell, attached to the stationary beam, measures the friction force F_t created between the hemisphere and the test specimen, as illustrated in Fig. 2(b). We have verified that the displacement of the suspension due to the friction force acting on the dimple is typically less than 10% of the displacement amplitude of the gimbal. Thus, the error committed in the measurement of the friction hysteresis loops using only one displacement measurement on the gimbal rather than two independent displacement measurements on the gimbal and the dimple, is small in the present study and can be neglected. It should be pointed out, however, that under high frictional load separate measurement of the displacement of both the dimple and the gimbal may be necessary to improve the accuracy of the friction hysteresis loops.

4. Test procedure and samples

We have used a regular stainless steel and laser polished stainless steel beam and hemisphere, and a stainless steel test specimen (flat plate). The laser polishing is a non-contact finishing technique where the surface topography is being smoothened by melting and vaporization of the top layer of the hemisphere material. Table 1 summarizes the surface and material properties for the hemisphere and test specimen we have used. The Young's modulus E was taken from the literature and hardness H was measured using a nano-indenter. The surface roughness properties were measured using an atomic force microscope. The measurements showed that the surface roughness of the dimple and gimbal is isotropic. Hence, the Greenwood–Williamson approach can be used to describe surface roughness of hemisphere and test specimen [14]. The average asperity tip radius ρ, the asperity density η, and the standard deviation of asperity summit heights σ_s can be obtained using the three spectral moments m_0, m_2, and m_4 of the surface roughness as described by McCool [15] (see appendix). The non-dimensional

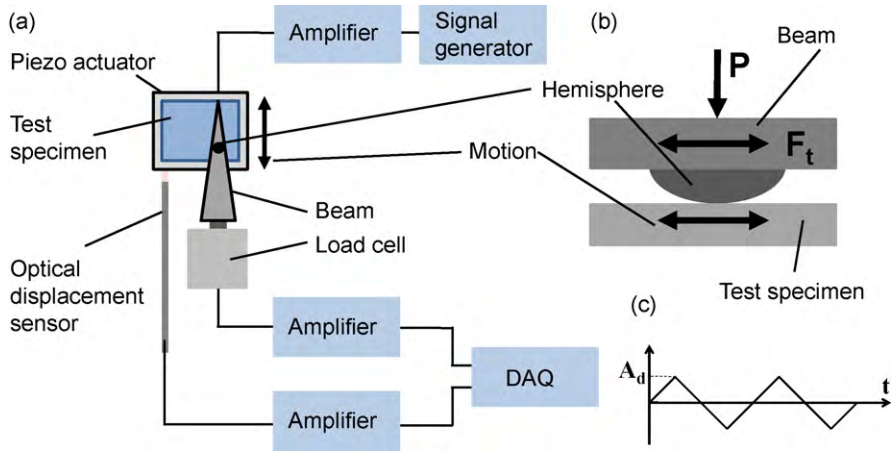

Fig. 2. (a) Schematic of experimental setup; (b) detailed side view of hemisphere/test specimen interface; and (c) displacement function.

Table 1
Material samples properties (before experiment).

Item	Material	ρ [nm]	η [nm^{-2}]	σ_s [nm]	σ_s/ρ	E [GPa]	H [GPa]
Flat plate	Stainless steel	6450.19	3.52E−07	42.86	6.64E−03	200.00	3.70
Hemisphere	Stainless steel	3314.42	1.02E−06	41.53	1.25E−02	200.00	3.92
Hemisphere	Laser polished stainless steel	78824.29	3.01E−08	28.39	3.60E−04	200.00	3.62

Table 2
Material sample combinations surface properties (before experiment).

Item	ρ [nm]	η [nm^{-2}]	σ_s [nm]	σ_s/ρ
Flat plate/hemisphere	2948.00	7.32E−07	59.89	2.03E−02
Flat plate/laser polished hemisphere	6428.71	3.29E−07	51.94	8.08E−03

value σ_s/ρ is a measure for the surface roughness. A low number (large ρ and small σ_s) indicates a smooth surface, and vice versa.

Table 2 shows the equivalent surface roughness parameters for two contacting rough surfaces [14].

From Tables 1 and 2 we note that the non-dimensional surface roughness (σ_s/ρ) of the laser polished hemisphere is two orders of magnitude smaller than the value for surfaces without laser polishing. The Young's modulus and hardness of the two materials are slightly different. Fig. 3(a) and (b) show a white light interferometry image of both hemispheres to illustrate the difference in surface roughness. Fig. 3(c) shows the flat surface. The scale indicates the z-height.

For each experiment a new hemisphere and test specimen was used. Each experiment was conducted five times and the results were averaged over all experiments. We have used a frequency of 1 Hz for the reciprocating motion of the test specimen, with a

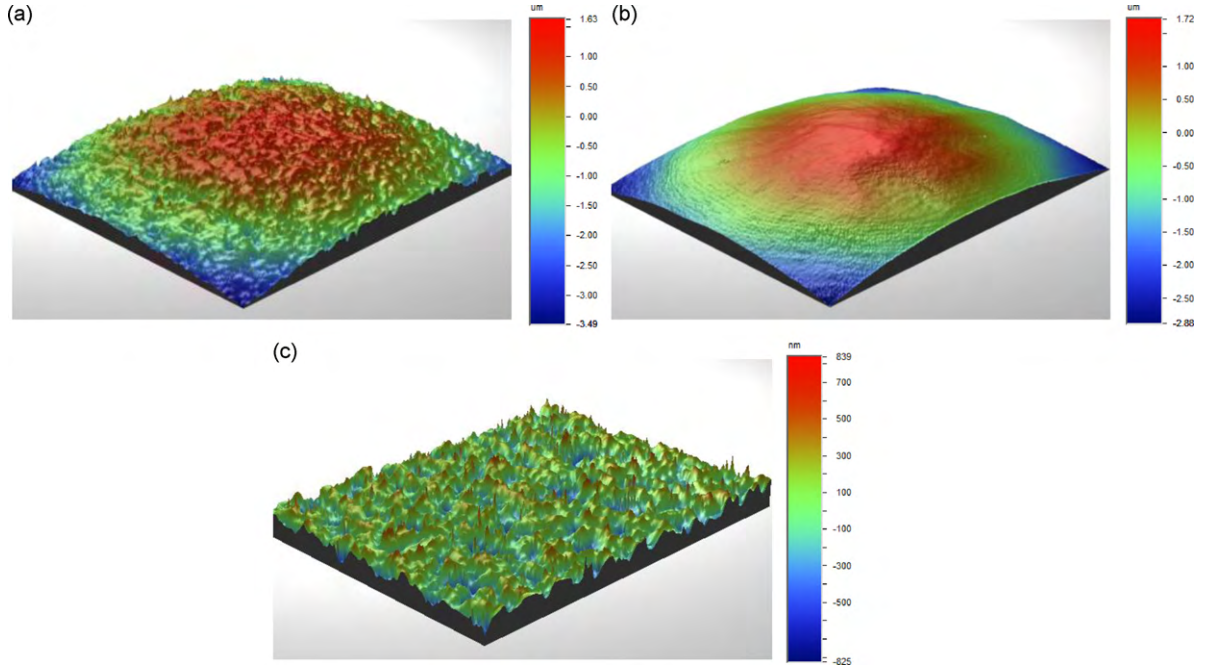

Fig. 3. White light interferometer image of (a) the regular stainless steel hemisphere, (b) the laser polished stainless steel hemisphere, and (c) the stainless steel flat surface (test specimen).

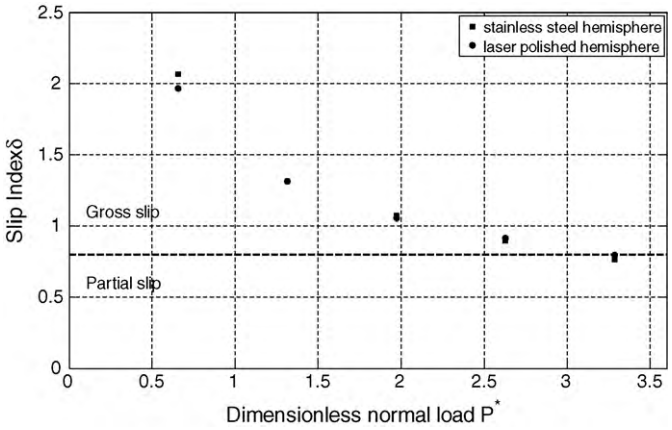

Fig. 4. Slip index versus dimensionless normal load for stainless steel and laser polished stainless steel hemisphere.

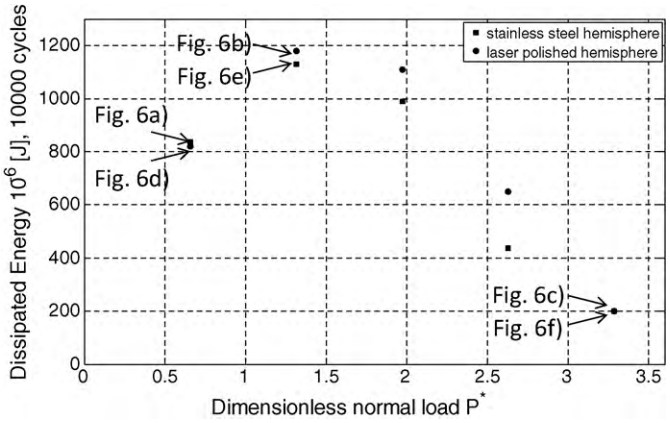

Fig. 5. Dissipated energy versus dimensionless normal load.

displacement amplitude $A_d = 3\,\mu$m. A normal load was applied to the hemisphere by adding a calibrated weight to the beam surface, directly over the hemisphere. We have used normal forces ranging between 10 and 50 mN. All tests ran for 10,000 cycles.

5. Results

In our experiments we have observed that the slip index stays approximately constant over a span of 10,000 cycles, i.e., the fretting regime remains invariable during the experiment. Based on this result it is justifiable to use the average slip index over all fretting cycles of one experiment when comparing different experiments with each other.

Fig. 4 shows the slip index as a function of the non-dimensional normal load, for the stainless steel and the laser polished stainless steel hemisphere. The horizontal dashed line at $\delta = 0.8$ indicates the transition from gross slip to partial slip. From Fig. 4 we observe that the slip index is the same for both cases. The dimensionless normal load P^* is defined as

$$P^* = \frac{P}{L_c} \tag{2}$$

with P the dimensional normal load and L_c the critical normal load at yield inception under stick conditions. It is convenient to define

$$L_c = \overline{L_c} P_c \tag{3}$$

where $\overline{L_c} = L_c/P_c$ is the ratio of the critical loads in full stick and perfect slip, given by [16]

$$\overline{L_c} = 8.88\nu - 10.13(\nu^2 + 0.089) \tag{4}$$

The critical load at yield inception under perfect slip conditions P_c is given by

$$P_c = \frac{\pi^3 Y_0}{6} C_\nu^3 \left(R(1-\nu^2)\left(\frac{Y_0}{E}\right)\right)^2 \tag{5}$$

where Y_0 is the yield strength, R is the radius, ν is the Poisson coefficient and E is the Young's modulus of the hemisphere [16]. C_ν is the ratio of maximum contact pressure under perfect slip condition at yield inception, and the yield strength, and is given by [16]

$$C_\nu = 1.234 + 1.256\nu \tag{6}$$

The slip index decreases monotonically as a function of the dimensionless normal load. We observe that the transition from gross slip to partial slip occurs at approximately $P^* = 3$.

Fig. 5 shows the dissipated energy as a function of dimensionless normal load after 10,000 cycles, for the stainless steel and the laser polished stainless steel hemisphere. The dissipated energy was calculated for each fretting cycle by determining the area contained within the friction hysteresis loop. Summing the energy for all cycles yields the total energy dissipated during the experiment. It has been shown by Fouvry et al. [17,18] and Yu et al. [19] that the dissipated energy during one fretting cycle is related to the wear produced during that cycle. From Fig. 5 we observe that the maximum energy dissipation occurs at $P^* = 1.3$, which is equivalent to a dimensional load of 20 mN in our experiment. The maximum is independent of the type of hemisphere, i.e., regardless of the surface roughness. We also note that the dissipated energy is slightly higher in the case of the laser polished hemisphere than in the case of the regular stainless steel hemisphere. The roughness of the laser polished hemisphere is two orders of magnitude smaller than the unpolished hemisphere. From Table 2 we observe that σ_s/ρ is significantly larger for the unpolished than for the laser polished hemisphere, which indicates that the asperities are smoother on the laser polished than the unpolished hemisphere, resulting in a larger real area of contact, i.e., more energy will be dissipated during fretting wear.

Fig. 6 shows optical microscope images of wear scars on the hemisphere after 10,000 fretting cycles under a dimensionless normal load of $P^* = 0.66$, $P^* = 1.31$ and $P^* = 3.29$, which is equivalent to a dimensional load of 10, 20 and 50 mN in our experiment. The wear scars for the respective (ascending) loads are given in Figs. 6(a)–(c) for the regular stainless steel hemisphere and in Figs. 6(d)–(f) for the laser polished stainless steel hemisphere. The corresponding energy dissipation data points are marked in Fig. 5.

We observe from Fig. 6 that more small wear particles are distributed at the periphery of the wear scar in the case of a laser polished hemisphere compared to a regular stainless steel hemisphere. We also observe that the size of the wear scar increases if the load is increased from $P^* = 0.66$ to $P^* = 1.31$. However, as the load is increased further, to $P^* = 3.29$, the wear scar decreases in size. Fig. 7 shows the corresponding friction hysteresis loops for the regular stainless steel hemisphere, i.e., friction force versus relative displacement. The slip amplitude A_s decreases with increasing normal load for constant displacement amplitude A_d. Very little slip occurs for a normal load of $P^* = 3.29$. Clearly, almost no energy is dissipated, since the area within the friction hysteresis loop (Fig. 7(c)) is nearly zero.

The optical microscope images of the wear scars in Fig. 6 show dark brown discoloration, suggesting that tribo-chemical processes occurred at the sliding interface. Energy-dispersive X-ray spectroscopy (EDX) analysis revealed the presence of a significant amount of oxygen in the wear scar, i.e., metal oxides are present in the wear scar.

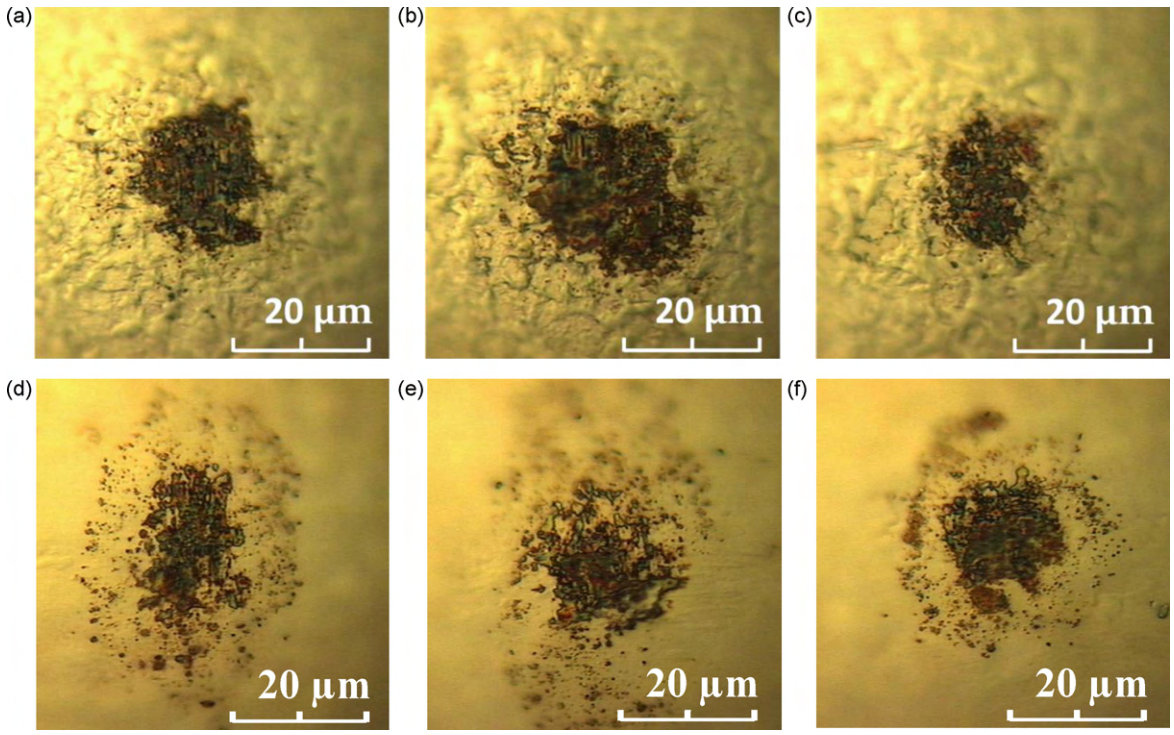

Fig. 6. wear scars after 10,000 fretting cycles under a non-dimensional normal load of $P^* = 0.66$, $P^* = 1.31$ and $P^* = 3.29$ for the regular stainless steel hemisphere (a–c) and for the laser polished stainless steel hemisphere (d–f).

6. Discussion

6.1. Surface roughness

Fig. 8(a) and (b) show white light interferometry images of the worn hemisphere surfaces, after 10,000 fretting cycles at a non-dimensional normal load of $P^* = 1.31$. Fig. 8(a) shows the regular stainless steel hemisphere. We observe that the roughness peaks have been worn off due to the reciprocating sliding contact. Asperities were flattened as a result of plastic deformation, and loose wear particles seem to have been generated from the hemisphere. Fig. 8(b) shows the laser polished stainless steel hemisphere for comparison. We observe that wear particles have been generated from the hemisphere surface, and that some of these particles have been re-deposited around the wear scar. The mating surfaces are shown in Fig. 8(c) and (d), respectively. Compared to the unworn surface in Fig. 3(c), we observe that asperities have been deformed. However, both surfaces shown in Fig. 8(c) and (d) look similar.

Fig. 9 shows a scanning electron microscope (SEM) image of the same wear scars as shown in Fig. 8(a) and (b). Fig. 9(a) shows the stainless steel hemisphere. Similar to Fig. 8(a), we observe that the roughness peaks in the wear scar have been flattened. Fig. 9(b) shows the laser polished hemisphere. The darker areas in the SEM image indicate recess areas on the hemisphere surface, identical to the ones observed in the white light interferometer image (Fig. 8(b)). Additionally, we observe a large amount of (sub) micrometer-sized particles adhering to the hemisphere surface. Small wear particles are also observed around the wear scar on the stainless steel hemisphere, but fewer than on the laser polished hemisphere.

The stainless steel and laser polished stainless steel hemisphere show a different wear mechanism, despite having experienced identical operating conditions. The difference appears to be related to the different surface roughness and hardness of both hemispheres, since all other parameters are identical. In the case of the regular stainless steel hemisphere, the hemisphere is harder and rougher than the flat test specimen (Table 1). Hence, the asperities on the hemisphere are plowing through the softer asperities on the flat. Therefore adhesive wear occurs and almost no abrasive wear is observed in Figs. 8(a) and 9(a). As a result, abrasive wear would be expected on the matching flat surface shown in Fig. 8(c). While some abrasive wear can be observed, we would have expected to see a larger wear scar. In the case of the laser polished hemisphere, the hemisphere is smoother and softer than the flat test specimen. Thus, the asperities of the flat are plowing through the softer asperities on the hemisphere, thereby creating abrasive wear on the hemisphere. This was clearly observed in Figs. 8(b) and 9(b).

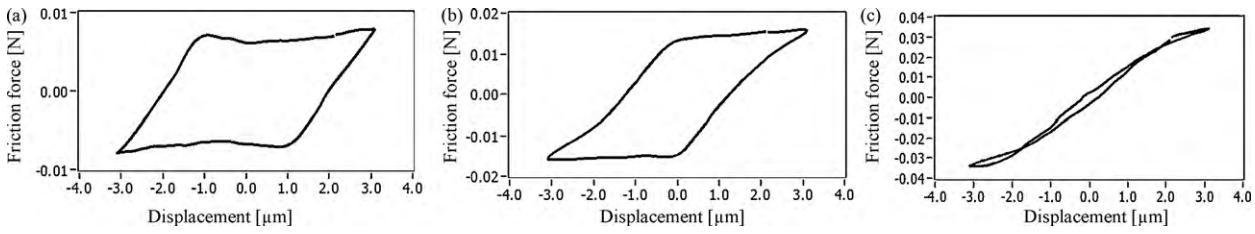

Fig. 7. Friction hysteresis loops for a stainless steel hemisphere under normal load of (a) $P^* = 0.66$, (b) $P^* = 1.31$, and (c) $P^* = 3.29$.

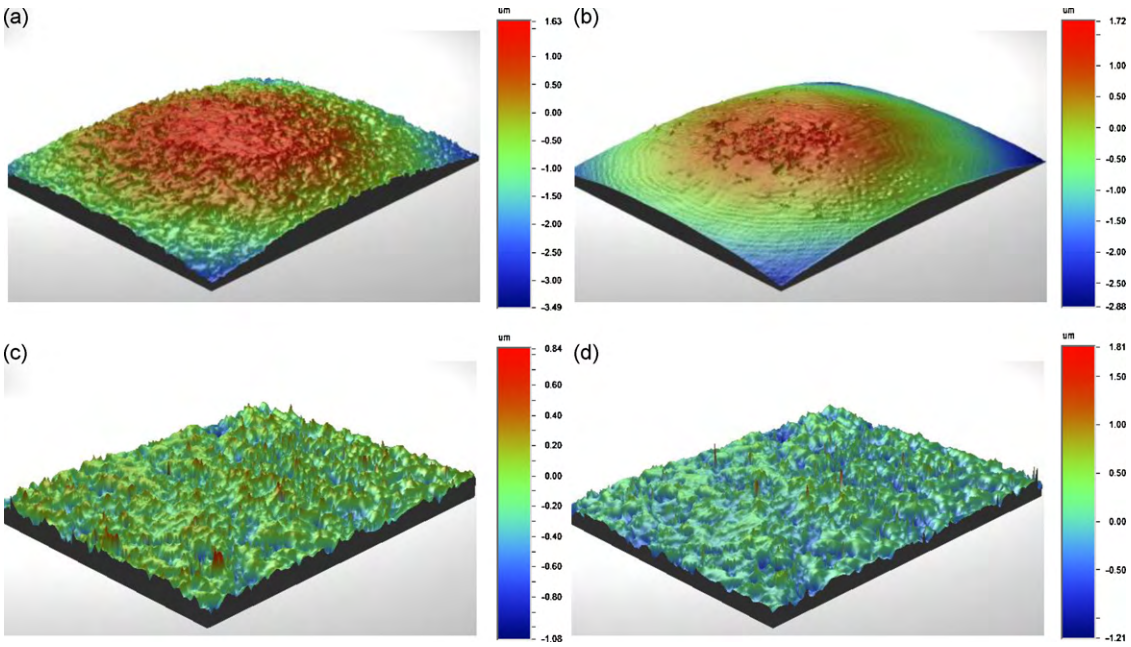

Fig. 8. White light interferometer image of the (a) worn stainless steel hemisphere, (b) worn laser polished stainless steel hemisphere, (c) flat surface after contact with stainless steel hemisphere and (d) flat surface after contact with laser polished stainless steel hemisphere.

Additionally, the stainless steel hemisphere has a surface roughness which is almost two orders of magnitude larger than the laser polished hemisphere. Therefore, the real area of contact between the hemisphere and the test specimen is significantly larger in the latter case. This may help clarify why more and smaller wear particles are formed around the wear scar of the laser polished hemisphere. The same normal load is distributed over a larger real contact area, resulting in smaller contact stresses between the contacting asperities on the hemisphere and flat, and, thus, smaller wear particles. Rabinowicz [1] showed that based on a balance between adhesive and elastic energy, wear particles need a minimum size to be released from a surface. Fig. 9(a) and (b) provide some evidence in support of this argument. In the case of the regular stainless steel hemisphere (Fig. 9(a)), wear particles too large to adhere to the hemisphere are formed at the interface as a result of higher contact stresses than in the laser polished case. These particles come loose and escape from the sliding interface into the environment. In the case of the laser polished hemisphere (Fig. 9(b)), smaller particles are generated, which adhere to the hemisphere at the boundaries of the wear scar, and are not released into the environment.

6.2. Comparison of results with Archard's wear law

It is interesting to compare our experimental results for the dissipated energy with Archard's wear equation for the regular stainless steel hemisphere. We define the equivalent sliding distance L_{eq} as

$$L_{eq} = 2\sum_{i=1}^{n} A_{s,i} \tag{7}$$

where $A_{s,i}$ is the sliding amplitude for fretting cycle i, and n is the total number of fretting cycles in the experiment. Archard's wear equation can then be written as [1]

$$\frac{V}{K} = \frac{L_{eq}P}{H} \tag{8}$$

where V is the wear volume, K is a wear constant which depends on the material combination, H is the hardness and P is the normal load. Fig. 10 shows the ratio of wear volume V and wear constant K versus the normal load. We observe from Fig. 10 that the shape of the curve is very similar to the shape of the curve shown in Fig. 4

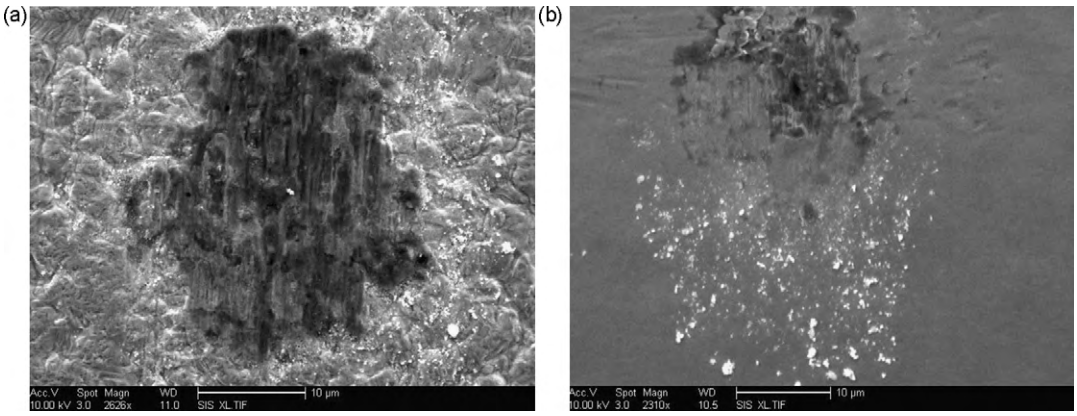

Fig. 9. Scanning electron microscope (SEM) images of the worn hemispheres after 10,000 cycles (a) stainless steel hemisphere and (b) laser polished stainless steel hemisphere.

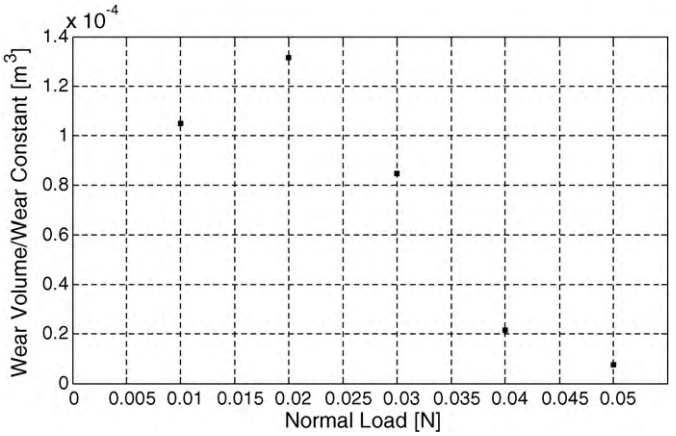

Fig. 10. Archard's wear law for an equivalent sliding distance.

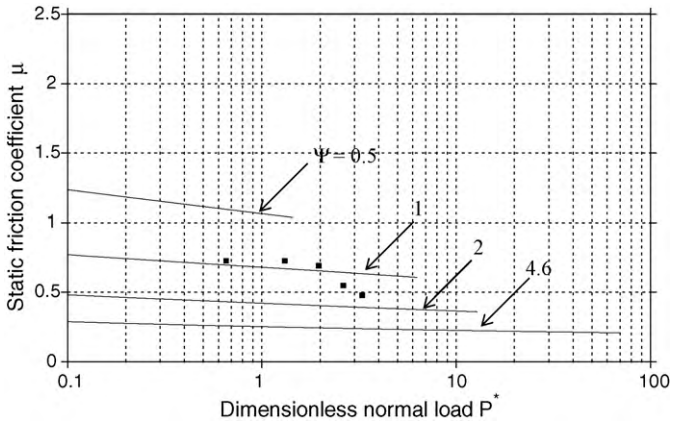

Fig. 11. Static friction coefficient versus dimensionless normal load.

for the dissipated energy versus the normal load. From Archard's equation, wear is proportional to load and sliding distance. Thus, the decrease in the wear scar size with increase in normal load is related to the decreased sliding distance at 50 mN. Clearly, less energy is dissipated at the 50 mN load case than at the 20 mN load since the sliding distance for each cycle is decreased substantially at the higher load.

The observation that fretting wear is consistent with Archard's wear equation, when taking into account an equivalent sliding distance, is remarkable. It also implies that reciprocating motion has the same effect with respect to wear generation than uni-directional sliding motion. Traditional wear literature mentions how wear is related to particle entrapment [1]. Uni-directional and reciprocating sliding result in different entrapment/escaping of particles from the sliding interface. In fact, one would expect the wear particles to escape from the sliding interface easier in the case of uni-directional sliding than in the case of fretting, resulting in more significant abrasive wear in the latter case. However, the net effect of both sliding regimes on wear volume appeared to be similar in our experiments. While we do not have a good explanation for this observation, one could speculate that in both uni-directional sliding and fretting, the wear particles escape from the sliding interface.

6.3. Comparison of our experimental data to existing contact mechanics models

In the literature only a few models are available that describe the contact between a rough sphere and a flat surface. Kogut and Etsion extended their contact model [20] for an elastic curved beam to include friction in compliant electrical connectors [21]. A more accurate model for elastic–plastic contact between two rough surfaces was developed in [16]. There the dimensionless normal load P^* and dimensionless maximum tangential load Q^*_{max} were found to be

$$P^* = \frac{2\pi\beta\psi^3}{(\bar{\delta})^{1.5}}\frac{\rho}{R}\int_0^R r^*\left[\int_{d^*}^{d^*+\delta_c^*}(z^*-d^*)^{3/2}\Phi^*(z^*)\,dz^*\int_{d^*+\delta_c^*}^{\infty}(z^*-d^*)^{3/2}(1-I(\alpha))\Phi^*(z^*)\,dz^*\right]dr^* \tag{9}$$

$$Q^*_{max} = \frac{2\pi\beta\psi^3}{(\bar{\delta})^{1.5}}\frac{\rho}{R}\int_0^R r^*\left[\int_{d^*}^{d^*+\delta_c^*}0.26(z^*-d^*)^{3/2}\coth\left(0.27\left((z^*-d^*)\frac{\psi^2\sigma/\sigma_s}{\bar{\delta}}\right)^{0.46}\right)\Phi^*(z^*)\,dz^*\right.$$
$$\left.+\int_{d^*+\delta_c^*}^{\infty}(z^*-d^*)^{3/2}(1-I(\alpha))\coth\left(0.27\left((z^*-d^*)\frac{\psi^2\sigma/\sigma_s}{\bar{\delta}}\right)^{0.46}\right)\Phi^*(z^*)\,dz^*\right]dr^* \tag{10}$$

where ψ is the plasticity index, Φ^* is a dimensionless Gaussian distribution function of asperity heights, z^* is the non-dimensional asperity height, d^* is the non-dimensional separation between hemisphere and test specimen (see *Nomenclature* for further parameter identification).

In Eqs. (9) and (10),

$$I = \exp\left[\left(1-\left((z^*-d^*)\frac{\psi^2\sigma/\sigma_s}{\bar{\delta_c}}\right)^{\alpha}\right)^{-1}\right]$$

and $\alpha = 0.174 + 0.08\nu$.

The static friction coefficient can then be obtained as

$$\mu = \frac{Q^*_{max}}{P^*} \tag{11}$$

Solving this model for the case of the regular stainless steel hemisphere yields the following result. Fig. 11 shows the static friction coefficient versus the dimensionless normal load (solid lines). We have used the parameters of Table 1, and have solved the model for a plasticity index of 0.5, 1, 2 and 4.6. The plasticity index of 4.6 represents the case of the regular stainless steel hemisphere prior to the experiment. The black square markers represent experimental data points, which show fair agreement with the model.

7. Conclusion

Based on our experiments, we have found that

(1) Fretting wear between a hemisphere and a flat surface is highly dependent on the normal load. Decreasing the normal load reduces the contact area and thus the wear volume. Increasing the normal load can cause the sliding interface to operate in the partial slip fretting regime, which causes a reduction in the generation of wear particles.

(2) Laser polishing of the hemisphere yields a significant reduction in surface roughness. However, no reduction in wear volume was observed. The results for dissipated energy indicate a slight increase in wear.
(3) The experimental results for the dissipated energy showed good agreement with Archard's wear law, when defining an equivalent sliding distance as the sum of the lengths of all sliding segments during the experiment. Our experiments also showed fair agreement with the more involved rough sphere/flat elastic plastic contact model.

Acknowledgements

We wish to thank Hanya-san and Edmund Fanslau from NHK international for supporting this research. We would also like to thank Professor Izhak Etsion, and Dr. Andrey Ovcharenko for their interest in this work, and Sebastian Helm and Dr. Ralf Brunner for help with some of the experiments.

Appendix A.

According to McCool's analysis [13], the spectral moments of a rough isotropic surface are given by

$$m_0 = AVG[y^2]$$
$$m_2 = AVG\left[\left(\frac{dy}{dx}\right)^2\right]$$
$$m_4 = AVG\left[\left(\frac{d^2y}{dx^2}\right)^2\right]$$

where $y(x)$ is the height distribution of the surface profile.

The radius of curvature of asperity heights, the areal density of the asperities and the standard deviation of asperity summit heights can be calculated as

$$r = 0.375\left(\frac{\pi}{m_4}\right)^{1/2}$$
$$\eta = \frac{m_4}{6\pi\sqrt{3}m_2}$$
$$\sigma_s = \left(m_0 - \frac{3.717\times10^{-4}}{\eta^2 r^2}\right)^{1/2}$$

For the case of two contacting isotropic rough surfaces 1 and 2, an equivalent rough surface in contact with a smooth flat can be defined. The spectral moments of this equivalent rough surface are given by summing the spectral moments of the individual surfaces. Hence,

$$m_i = (m_i)_1 + (m_i)_2$$

where $i = 0, 2, 4$.

References

[1] E. Rabinowicz, Friction and Wear of Materials, Wiley-Interscience, New York, 1995.
[2] R.B. Waterhouse, Fretting Corrosion, Pergamon, Oxford, 1972.
[3] I.-M. Feng, B.G. Rightmire, The mechanism of fretting, Lubrication Eng. 9 (1953) 134–136, 158–161.
[4] Y. Berthier, L. Vincent, M. Godet, Fretting fatigue and fretting wear, Tribol. Int. 22 (1989) 235–242.
[5] P.L. Hurricks, The mechanism of fretting – a review, Wear 15 (1970) 389–409.
[6] W.E. Campbell, The current status of fretting corrosion, Symp. Fretting Corrosion, ASTM Spec. Techn. Publ. 4 (1953) 3.
[7] J.T. Demasimarcin, D.K. Gupta, Protective coatings in the gas-turbine engine, Surf. Coat. Technol. 68 (1994) 1–9.
[8] O. Vingsbo, S. Soderberg, On fretting maps, Wear 126 (1988) 131–147.
[9] S. Fouvry, Ph. Kapsa, L. Vincent, Analysis of sliding behavior for fretting loadings: determination of transition criteria, Wear 185 (1995) 35–46.
[10] G.X. Chen, Z.R. Zhou, Study on transition between fretting and reciprocating sliding wear, Wear 250 (2001) 665–672.
[11] M. Varenberg, I. Etsion, G. Halperin, Slip index: a new unified approach to fretting, Tribol. Lett. 17 (3) (2004) 569–573.
[12] M. Varenberg, I. Etsion, G. Halperin, Nanoscale fretting wear study by scanning probe microscopy, Tribol. Lett. 18 (2005) 493–498.
[13] H. Mohrbacher, J.P. Celis, J.R. Roos, Laboratory testing of displacement and load induced fretting, Tribol. Int. 18 (5) (1995) 269–278.
[14] J.A. Greenwood, J.B.P. Williamson, Contact of nominally flat surfaces, Proc. R. Soc. Lond., Ser. A 295 (1966) 300–319.
[15] J.I. McCool, Relating profile instrument measurements to the functional performance of rough surfaces, J. Tribol. Trans. ASME 109 (1987) 264.
[16] D. Cohen, Y. Kligerman, I. Etsion, The effect of surface roughness on static friction and junction growth of an elastic–plastic spherical contact, J. Tribol. Trans. ASME 131 (2009) 021404.
[17] S. Fouvry, Ph. Kapsa, L. Vincent, Quantification of fretting damage, Wear 200 (1996) 186–205.
[18] S. Fouvry, C. Paulin, S. Deyber, Impact of contact size and gross-partial slip conditions on Ti–6Al–4V/Ti–6Al–4V fretting wear, Tribol. Int. 42 (2009) 461–474.
[19] J. Yu, L. Qian, B. Yu, Z. Zhou, Nanofretting behavior of monocrystalline silicon (1 0 0) against SiO_2 microsphere in vacuum, Tribol. Lett. 34 (2009) 31–40.
[20] L. Kogut, I. Etsion, The contact of a compliant curved and a nominally flat rough surface, Tribol. Trans. 43 (2000) 507–513.
[21] L. Kogut, I. Etsion, Electrical conductivity and friction force estimation in compliant electrical connectors, Tribol. Trans. 43 (2000) 816–822.